Article

Wettability Study of an Acidified Nano-TiO$_2$ Superhydrophobic Surface

Xiaoru Hao,* Zhihao Cheng, Yu Zhang, Jun Xie, Haikun Zheng, Chunxiao Yue, and Wei Sheng

Cite This: ACS Omega 2024, 9, 4447−4454

Read Online

ACCESS | ▥ Metrics & More | ▦ Article Recommendations

ABSTRACT: The operation of aerospace equipment is often affected by icing and frosting. In order to reduce the loss caused by icing in the industrial field, it is an effective method to prepare superhydrophobic coatings by modifying nanoparticles with low surface energy materials. In order to explore a method of preparing a superhydrophobic surface that can be popularized, a two-step spraying method was employed to create a superhydrophobic coating. The surface was characterized by Fourier transform infrared spectroscopy (FTIR) and field emission scanning electron microscopy (SEM). The optimal preparation process was obtained by analyzing the surface contact angle data. The results showed that stearic acid was grafted onto the surface of TiO$_2$ by esterification reaction. The existence of long methyl and methylene hydrophobic groups in the tail of the stearic acid molecule made the modified TiO$_2$ hydrophobic. It is verified that water molecules have strong adsorption on the surface of unmodified TiO$_2$. Stearic acid molecules can reduce the interfacial energy in the system.
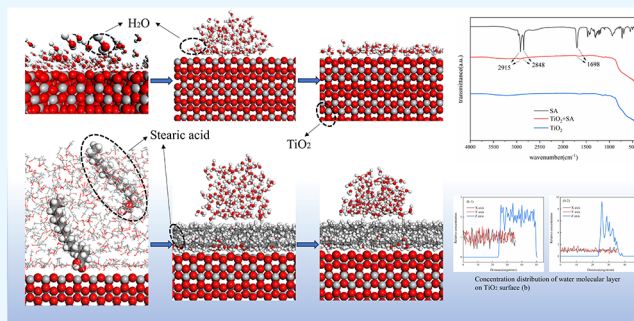
1. INTRODUCTION

Various superhydrophobic phenomena widely exist in our life. Generally, contact angles higher than 150° and rolling angles lower than 5° are called superhydrophobic surfaces.[1,2] Inspired by the superhydrophobic phenomenon in life, in recent years, more and more scientific researchers have carried out research on superhydrophobic surfaces.[3−5] Because of its special contact behavior, it is widely used in various fields, including corrosion prevention,[6,7] self-cleaning,[8,9] antifouling,[10,11] and deicing.[12,13] Research shows that surface heterogeneity and roughness are two important factors that constitute superhydrophobic properties.[14,15] Generally speaking, it is the most common method to combine low surface energy materials and micro/nano structures to obtain superhydrophobic surfaces.

Up to now, many researchers have used different methods to construct superhydrophobic surfaces, including vapor deposition,[16] electronic etching,[17] sol−gel process,[18,19] and phase separation.[20] In these methods, the surface roughness is first obtained by using tools and then modified by using low surface energy substances. He et al.[21] used silane coupling agent KH-570 to organically modify the inorganic filler titanium dioxide (TiO$_2$) on the glass substrate. The hydrophobicity and dispersion of the modified TiO$_2$ particles were enhanced, and the hydrophobic effect was the best when the mass fraction of KH-570 was 15%. Yang et al.[22] used stearic acid as a low surface energy modifier to modify the surface of TiO$_2$ and cellulose nanofiber composites (CNF). The surface of the CNF was coated with TiO$_2$. Because the surface of CNF was

rich in hydroxyl groups, it could be connected with the hydroxyl groups on the surface of TiO$_2$ by hydrogen bonding. TiO$_2$ promoted the nucleation and further growth of the CNF surface. Stearic acid (SA) removed hydrophilic hydroxyl groups in the TiO$_2$/CNF system and introduced hydrophobic alkyl groups. The TiO$_2$/CNF composite has a nano scale rough structure on the surface, which makes it superhydrophobic. However, most of the above methods for preparing superhydrophobic surfaces are complex and have a variety of materials, which is not conducive to wide development of the preparation process.

Limited by many harsh requirements of experimental research, with the increasing progress of computer development, researchers began to apply molecular dynamics to the field of superhydrophobic and gradually became a new trend,[23,24] that is, to study the interaction between interfaces at the micro level through molecular dynamics simulation and analyze the interaction mechanism between droplets and superhydrophobic surfaces to understand the wettability of surfaces.[25,26] Werder et al.[27] simulated the behavior of liquid

droplets in different carbon nanotube (CNT) radii. The contact angle of liquid droplets on the CNT surface in the simulation system was calculated as a function and compared with the experimental observation results of Gogotsi et al.,[28] and it was concluded that the interface has non wetting behavior. Rui et al.[29] studied the diffusion effect of water molecules on the coal surface with different degrees of coalification. In the simulation, the change of the contact angle is consistent with the experimental results. The research results show that the increase of oxygen-containing functional groups leads to a decrease of the contact angle. The hydrogen bond formed between water molecules and coal provides an important contribution to the diffusion effect of water droplets on the coal surface. Although these studies have analyzed the superhydrophobic phenomenon at the microscopic level, there is less analysis of the specific units that play a role in this hydrophobic effect and the functional groups in the molecular chain are ignored.

Nanomaterials ensure the construction of micronano structures on superhydrophobic surfaces. In recent years, research on superhydrophobic coatings based on TiO_2 nanoparticles has attracted much attention. As a common nanomaterial, TiO_2 nanoparticles are one of the ideal superhydrophobic materials for constructing nanoscale rough structures. It is low cost, is easy to obtain, and has a wide range of applications. Therefore, in this paper, superhydrophobic surfaces were prepared by a two-step spraying method using SA and nano-TiO_2 particles with low surface energy as raw materials. The simulation model was constructed based on the experimental materials, and the crystal structure was constructed based on the first principle of molecular dynamics. The bonding relationship between TiO_2 and SA was analyzed by density functional theory under the conditions of classical Newtonian mechanics, which was compared with the experimental results of infrared characterization. At the same time, the superhydrophobic phenomenon of water molecules on the surface of TiO_2 molecules grafted with SA molecules was studied at the molecular level, which provided a basis for the study of microwettability and the analysis of macro-wettability of superhydrophobic coatings and explored a scalable preparation method of superhydrophobic coatings.

2. MATERIALS AND METHODS

2.1. Experimental Materials. Nano-TiO_2 powder with a particle size of 20 nm was purchased from Hebei Chuancheng Metal Materials Co., Ltd. SA, acetone (analytically pure AR), and anhydrous ethanol (mass fraction ≥99.7%) were purchased from Shanghai Aladdin Biochemical Technology Co., Ltd. Epoxy resin (mass fraction 98%) and polyamide resin (curing agent) were purchased from Hangzhou Wuhui Port Co., Ltd.

2.2. Experimental Equipment. Equipment used for this study were a KQ3200DE magnetic ultrasonic cleaner (Shanghai Shiyan Equipment Co., Ltd.), ZK-FA210 electronic balance (Metler-Toledo International Co., Ltd.), ZX-9140MBE electric heating constant temperature blower dryer (Wuxi Marite Technology Co., Ltd.), 0.8 cm-caliber W-71 spray gun (Nantong Jiehao Machinery Tool Co., Ltd.), merlin compact scanning electron microscope (Beijing Prysies Instrument Co., Ltd.), WQF-520 Fourier infrared spectrometer (Tianjin Energy Spectrum Technology Co., Ltd.), and optical contact angle (CA) measuring instrument (Shanghai Xuanzhun Instrument Co., Ltd.).

2.3. Preparation of a Nano-TiO_2/SA Superhydrophobic Surface. In order to prepare a kind of superhydrophobic surface with wide application and high feasibility, this experiment set up one-step spraying group A and two-step spraying group B and another blank group for comparative experiment. In group A, a certain amount of TiO_2 was added to 20 mL of ethanol for ultrasonic dispersion for 0.5 h and then 3 wt % SA was added for magnetic stirring for 1 h to fully react. Subsequently, 1 g of epoxy resin and curing agent B were added to the reaction reagent at a ratio of 1:1 and magnetically stirred for 1 h. The dispersed coating was uniformly sprayed onto the glass surface by a spray gun. After that, the hydrophobic coating was cured at 80 °C for 4 h and room temperature for 2 h in a blast drying oven to obtain a one-step sprayed hydrophobic coating. In the experiment of group B, 1 g of epoxy resin and curing agent were dissolved and dispersed in 20 mL of ethanol at a ratio of 1:1, sprayed on the glass slide substrate, and dried at 60 °C for 0.5 h in a blast drying oven. Subsequently, the modified reagent was sprayed on the substrate, cured at 80 °C for 4 h, and cured at room temperature for 2 h to obtain a two-step sprayed hydrophobic coating.

2.4. Molecular Dynamics Simulation. The shortcoming of molecular dynamics simulation is that it can only simulate the motion of a short time. For the case of a large number of atoms or an infinite system, the calculation ability is far from enough, the calculation time cost is high, and the interaction force between the atoms and the internal atoms is quite different. Therefore, periodic boundary conditions are introduced according to the shortcomings of the calculation. The content of the periodic boundary condition is that there are numerous identical mirrors around the system and the middle is the unit to be simulated. The unit lattice is composed of 3 × 3 × 3 types and belongs to the three-dimensional model. The role of periodic boundary conditions is to continuously replicate the elements that need to be simulated in the surrounding direction and obtain an infinite system to describe the macroscopic system after infinite replication. In the simulation process, if an atom moves from the simulation unit to the outside of the unit lattice, the mirror unit in the opposite direction will have the same atom entering the simulation unit so that the number and density of atoms in the system remain unchanged.

The system model is constructed under periodic boundary conditions. All simulation processes are calculated under the Forcite program and Compass force field. The force field can simulate the structure, vibration frequency, and thermodynamic properties of isolated molecules and can simulate the structure and properties of condensed matter more accurately. The model construction mainly includes an anatase $TiO_2(001)$ crystal plane, a SiO_2 crystal plane, and an SA $(CH_3(CH_2)_{16}COOH)$ molecule, and the interface model is optimized by the steepest descent method (convergence standard is 1000 kcal/mol) and the conjugate gradient method (convergence standard is 10 kcal/mol) for a maximum of 20,000 steps. Under periodic boundary conditions, the interaction force is calculated by the Velocity-Verlet algorithm. The algorithm can give the particle position, velocity, and force at the same time and ensure the calculation accuracy. In the simulation process, an NVT ensemble is used, the temperature is controlled by nose thermostat at 298 K, the time step is 1.0 fs, and the lattice parameter of the SiO_2 crystal surface instead of glass surface is 57 Å × 57 Å × 90 Å. Insert 30 SA molecules

were inserted near the surface of $TiO_2(001)$. After balancing for 300 ps under the NVT ensemble, a layer of graphite sheet is placed on the SA molecular layer along the Z axis and the graphite sheet is fixed as close to the molecular layer as possible. The graphite sheet is removed, and the model system is dynamically relaxed for 500 ps to ensure the structural stability, after geometric optimization for many times until the surface is smooth. The adsorption process of SA molecules and the movement of the water layer composed of 500 water molecules on the TiO_2 surface and SiO_2 surface are simulated at the time step of 300 ps. Nano water droplets with a radius of 1 nm are constructed to simulate their dynamic motion on the TiO_2 surface and SA molecular layer.

3. RESULTS AND DISCUSSION

3.1. Surface Wettability Analysis. Under the dosage of 3 wt % SA in Table 1, the CA of group A sprayed in one step

Table 1. Sample Preparation and Contact Angle

group	TiO₂ dosage (g)	dry	CA (°)
A	0.1	no	99.93
	0.2	no	124.99
	0.3	no	152.85
	0.4	no	106.70
B	0.3	yes	153.15
	0.4	yes	108.00

increases with the increase of the mass fraction of TiO_2. When the addition amount of TiO_2 is 0.3 g, the CA reaches the highest point, which is 152.85°, and when the addition amount increases to 0.4 g, the CA is 106.70°. Consequently, in group B of two-step spraying, the addition amount of TiO_2 is 0.3 and 0.4 g. The results show that the optimal experimental scheme is when the addition amount of TiO_2 is 0.3 g in two-step spraying.

The hydrophobic effect of the prepared surface was explored by changing the amount of TiO_2 (0.1, 0.2, 0.3, 0.4 g). The change trend and imaging diagram of CA are shown in Figure 1. It can be seen from Figure 1b that the blank group showed strong hydrophilicity due to the smoothness of the glass and the large number of hydroxyl groups attached to the glass surface in the air. The CA was 59.04°, and the surface was completely wetted after a period of time. When the surface is sprayed with a layer of modified nano-TiO_2 particles, SA reacts with the −OH and −COOH groups on the surface of nanoparticles, that is, esterification reaction, leaving a long −CH_2 chain as the tail, making the surface hydrophobic. With the increase of TiO_2 addition, the surface is completely covered by hydrophobic long chains. After the addition amount of TiO_2 was increased to 0.4 g again, SA was not enough to modify the nanoparticles, so the hydrophobic effect decreased. The experimental results of 0.4 g of TiO_2 addition in group B also began to decrease the CA, which proved that too much TiO_2 addition will affect the hydrophobicity. For the sake of experimental efficiency, in the two groups, it is more appropriate to add 0.3 g of TiO_2 in group B and bake for 1 h.

As shown in Figure 1d, the droplets directly penetrate and spread on the surface of the unmodified TiO_2 surface while the droplets on the modified TiO_2 surface exhibit a nearly circular shape with a high CA. The results showed that TiO_2 without SA modification showed strong hydrophilicity while the surface of the modified TiO_2 showed good hydrophobicity after SA
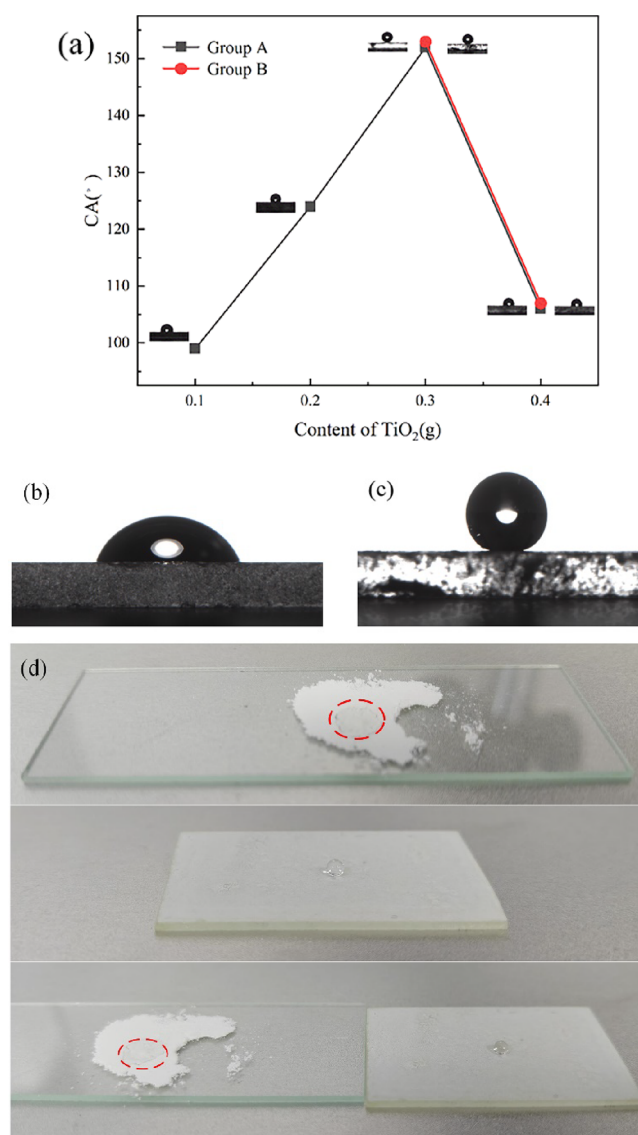

Figure 1. Schematic diagram of CA change (a), CA imaging diagram of blank group (b), and optimal group CA imaging (c). (d) Comparison of an unmodified TiO_2 surface and a modified TiO_2 surface.

modification. This also indirectly proves that SA successfully modified the nano-TiO_2 particles.

3.2. Prepared Surface Characterization. *3.2.1. Micro Morphology Analysis of Nano-TiO_2 Particles.* In order to explore the hydrophobic mechanism of the prepared superhydrophobic surface, the micro morphology of nano-TiO_2 particles was characterized by SEM in Figure 2. Spherical
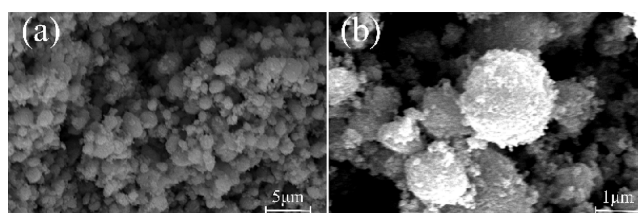

Figure 2. (a) Micromorphology of TiO_2 nanoparticles. (b) High-rate microstructure of TiO_2 nanoparticles.

TiO$_2$ particles were analyzed under a scanning electron microscope with magnification of 5 and 1 μm. In this experiment, the particle size of TiO$_2$ was 20 nm. However, it can be found in the figure that the nanoparticles were not uniform and there was agglomeration. This is because the TiO$_2$ particles exposed to the air have high surface energy and the surface area is large under the elliptical shape, which promotes the aggregation.

The roughness section depth of the coating surface is shown in Figure 3a, with the highest peak value of 3.37 μm and the
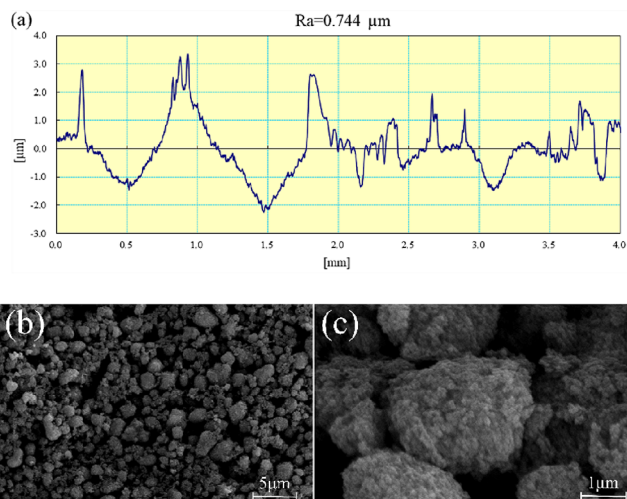

Figure 3. Depth roughness of the coating surface (a). Micromorphology of the superhydrophobic TiO$_2$ surface (b). High-rate microstructure of superhydrophobic TiO$_2$ surface (c).

lowest valley value of -2.24 μm. The section Ra value measured within the length of 4 mm of the surface is 0.744 μm. The surface morphology of nano-TiO$_2$ particles modified by SA is shown in Figure 3b,c. Compared with Figure 2, the shape of TiO$_2$ has not changed but the surface is more uniform as a whole. Most particles are about 25 nm in diameter, and there are a lot of gaps between the particles, so air can fill them. Under the action of SA, a low surface energy material, the agglomeration of TiO$_2$ particles is prevented and the surface free energy is reduced.

3.2.2. Fourier Transform Infrared Spectroscopy (FTIR) Analysis. Characteristic groups on the TiO$_2$ surface were analyzed by FTIR. In Figure 4, the absorption peaks of SA appeared at 2915 and 2848, corresponding to the stretching vibration peaks of the C−H bond in −CH$_3$ and −CH$_2$, respectively. The absorption peak also appeared in the TiO$_2$/SA spectrum at the same position, indicating that SA had been linked to the surface of the TiO$_2$ particles. The absorption peaks at 1698 on these two spectral curves correspond to the stretching vibration of the C=O bond in the −COOH group, indicating that SA was grafted onto the surface of TiO$_2$ by esterification reaction between the carboxyl group of the SA molecule and the hydroxyl group on the surface of TiO$_2$. The existence of long methyl and methylene hydrophobic groups in the tail of SA makes the modified TiO$_2$ hydrophobic.

3.2.3. Delayed Icing Experiment on a Superhydrophobic Surface. The delayed icing test tested the icing of 5 μL droplets on two surfaces at -10 and -15 °C. Because icing is affected by ambient temperature and humidity, the ambient air humidity is maintained at 68%, each group of tests is set five
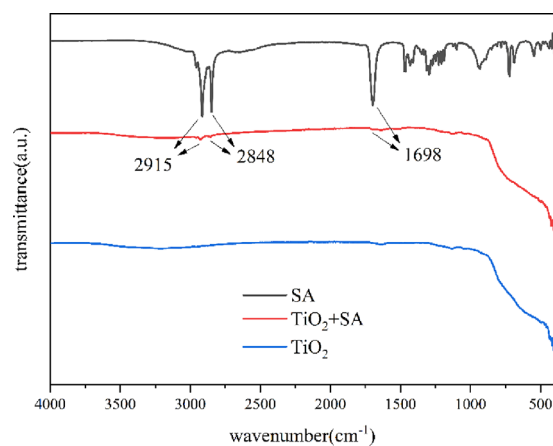
Figure 4. Fourier infrared spectrum curve.

times, and the average value is taken as the final experimental data.

Figure 5 records the delayed icing process of droplets on two surfaces. It can be found that no matter what kind of surface
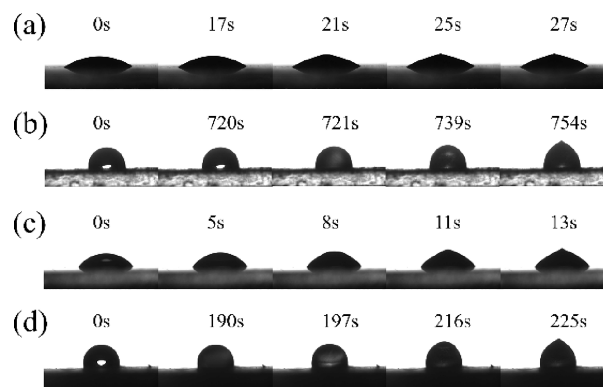
Figure 5. Icing process of an ordinary glass carrier (a) and a TiO$_2$/SA superhydrophobic surface (b) at -10 °C. Icing process of an ordinary glass carrier (c) and a TiO$_2$/SA superhydrophobic surface (d) at -15 °C.

the droplet is on, it is completely divided into two stages, from the beginning to the icing. For the first stage, first, the droplet exchanges heat with the surrounding atmosphere under the action of the ambient temperature. When the droplet surface is cooled to 0 °C, due to the crystal nucleus being more likely to appear on the solid/liquid/gas three-phase contact surface, the droplet begins to undergo heterogeneous nucleation in a very short time. For the second stage, the ice layer of nucleation and crystallization gradually grows up from the bottom contact interface. Finally, the droplet completely freezes and expands in volume. When the ambient temperature is -10 °C, the droplet cooling time on the surface of the ordinary glass slide is 17s and the time required for complete icing is 10 s. On the TiO$_2$/SA superhydrophobic surface, the droplet cooling time is 721 s, the time required for complete icing is 33 s, and the icing is delayed by 17 times.

In order to study the influence of different temperatures on the icing time, an icing test at -15 °C was set up. It can be found that after many tests, when the ambient temperature is reduced to -15 °C, the droplets on the surface of the ordinary glass slide are frozen, the cooling time is very short, and the freezing time is 13 s; the delayed icing time of the TiO$_2$/SA

superhydrophobic surface is 225 s. The above results show that the TiO₂/SA superhydrophobic coating exhibits fairly good anti-icing ability.

3.3. Molecular Dynamics Simulation Analysis.
3.3.1. Hydrogen Bond Analysis and SA Adsorption Model. The mechanism of SA-modified TiO₂ nanoparticles was determined by molecular dynamics simulation. In the simulation system, hydrogen bonds are generated among water molecules in the water layer and between water molecules and TiO₂ crystals. Studies have shown that the hydrogen bond length is 1.1−2.5 Å,[30,31] As shown in Figure 6a,
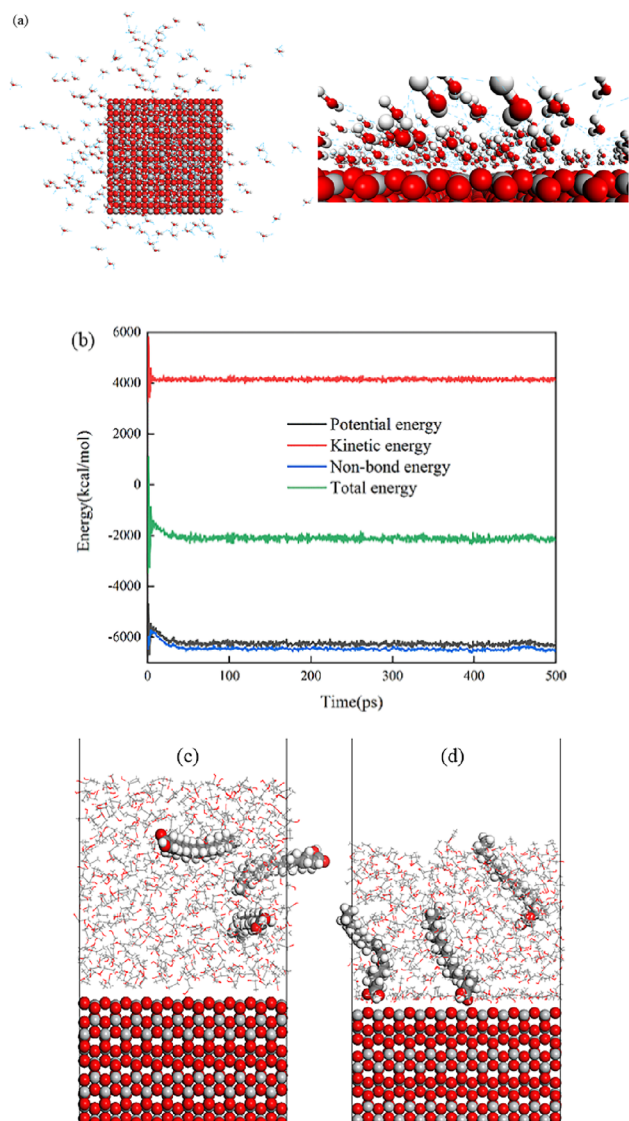
Figure 6. (a) Hydrogen bonds in the model. SA adsorption simulation: (b) energy changes. (c) Initial state. (d) Adsorption state.

the motion process of the water molecular layer on the TiO₂ surface is simulated. Hydrogen bonds formed between water molecules and water molecules and between water molecules and TiO₂ after the 300 ps simulation step. The average hydrogen bond length between water molecules is 2.16 Å, and the average hydrogen bond length between water molecules and TiO₂ is 2.41 Å, both within a reasonable range, which proves the correctness of the model in this paper.

The adsorption behavior of three SA molecules on the TiO₂ crystal was simulated in ethanol solution. Figure 6b shows that the energy of the model system tends to be minimized after 500 ps of simulation and the solution is in equilibrium. Random distribution of SA molecules in solution at the initial state is shown in Figure 6c. Under the COMPASS force field, due to the adsorption of TiO₂ on the surface molecules, SA molecules change from being in a free state to being adsorbed on the TiO₂ surface, the alkyl chain in the molecule is nearly vertical, and the tail is far from the surface, as shown in Figure 6d.

3.3.2. Analysis of Water Molecule Concentration Distribution on the SiO₂/TiO₂ Surface. Figure 7 demonstrates the concentration distribution of the water molecular layer on the surface of SiO₂ and TiO₂ and analyzes the influence of adsorption on the movement characteristics of the water molecular layer. On the Z axis, it can be seen from Figure 7a-1 that the initial water molecules of the model were distributed in the range of 20−50 Å from the surface of SiO₂. Under the nonbonding force, the water molecular layer was adsorbed to 20−30 Å from the surface after 300 ps movement (Figure 7a-2) and the maximum concentration was 8.70. In Figure 7b-1,b-2, when the water layer on the surface of TiO₂ reaches the equilibrium state, the maximum concentration curve is located at 25 Å away from the surface and there are still water molecules at 24−40 Å, which proves that the hydrophilicity of the SiO₂ surface is slightly stronger than that of the TiO₂ surface. At the same time, on both surfaces, water molecules in the X and Y axes fluctuate only in a fixed, small range.
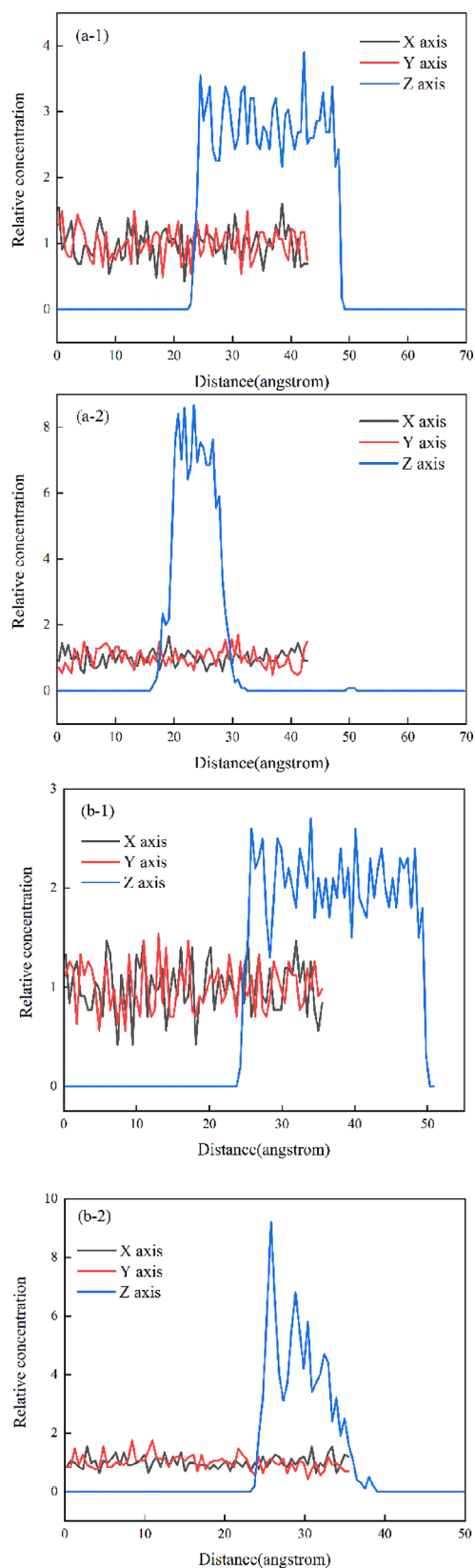
3.3.3. Root Mean Square Displacement and Diffusion Coefficient. Water droplets with a radius of 1 nm were further constructed to simulate the wetting process on the TiO₂ surface and the SA molecular acidification surface. After the dynamic simulation of 300 ps time step, the energy of the two models is stable and no violent fluctuation is observed, which proves that the model reaches the equilibrium state. The mean square displacement of nanowater molecular clusters is used to illustrate the molecular trajectory. As shown in Figure 8, during the process from the initial state to the equilibrium state, the mean square displacement of water molecular clusters on the TiO₂ surface is almost twice larger than that on the acidification surface of the SA molecule, indicating that water molecular clusters have high activity and a wide displacement range on their surfaces. Second, the diffusion coefficient of water molecular clusters can be expressed by the fitted function of root-mean-square displacement, and the formula is as follows:

$$D = \frac{1}{6Na} \lim_{x \to \infty} \frac{d}{dt} \sum_{i=1}^{Na} \langle [r_i(t) - r_i(0)]^2 \rangle \tag{1}$$

In the formula, D is the diffusion coefficient, Na denotes the number of molecules, r denotes the position of molecules at a certain moment, and t denotes the time step.
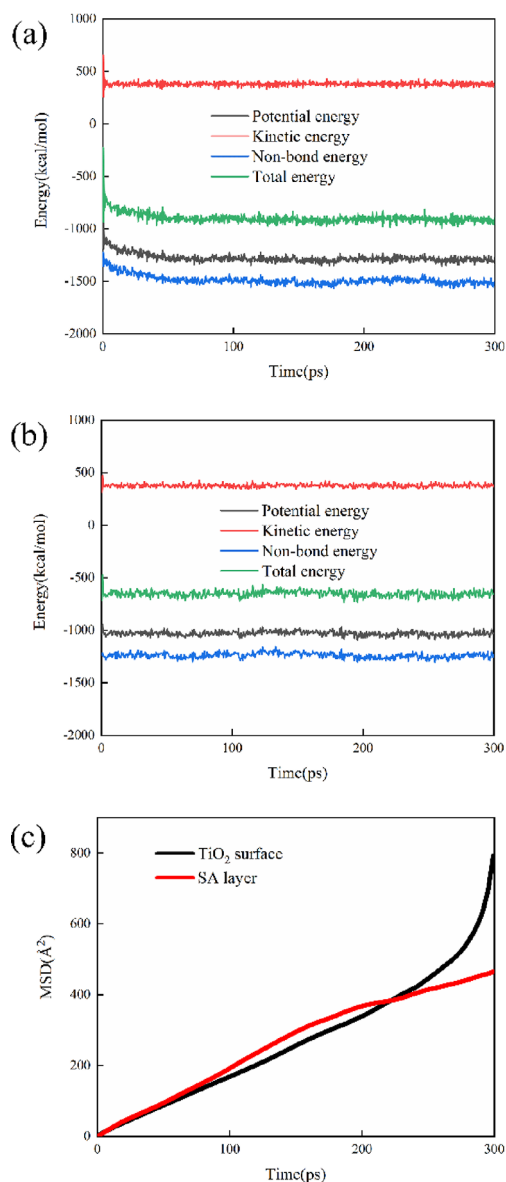
After fitting, the function of water molecular clusters on the TiO₂ surface and acidified surface is $Y_1 = 1.95X - 21.47$, $Y_2 = 1.58X + 28.86$, respectively. D_1 and D_2 are 3.25×10^{-9} and 2.63×10^{-9} m²/s, respectively. The smaller diffusion coefficient of the acidified surface means a weaker diffusion effect and smaller mobility of water molecular clusters.

Figure 9 shows the specific conformation of water molecules on the TiO₂ surface (a) and acidified surface (b) during the simulation process. Within a fixed time step, the droplets on
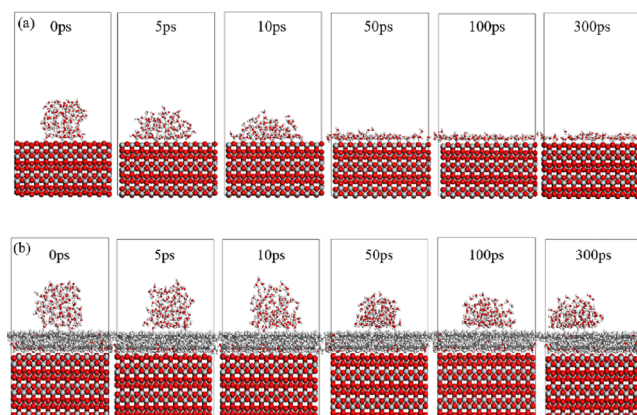
Figure 8. Energy change of acidified surface composed of the TiO_2 surface (a), SA molecule (b), and mean square displacement (c).

Figure 7. Concentration distribution of the water molecular layer on the SiO_2 surface (a)/TiO_2 surface (b).

Figure 9. Wetting process of water droplets on TiO_2 (a) and SA (b) acidified surfaces.

the TiO_2 surface quickly spread and cover the surface while the droplets on the acidified surface still remain elliptical after a series of bounces, which indicates that SA molecules

successfully modify TiO_2 from hydrophilicity to hydrophobicity.

3.3.4. Interaction Energy between SA Layer and Water Cluster, TiO_2 Surface, and Water Cluster Model System. The acidification surface was constructed by optimized SA molecules. The adsorption layer was a water molecular cluster. After the adsorption layer reached equilibrium with the substrate surface, the interaction energy of the two model systems of the SA layer-water cluster and the TiO_2 surface water cluster was calculated, respectively. The calculation formula is as follows:

$$E = \frac{(E_{total} - E_{surface} - E_{polymer})}{S} \qquad (2)$$

Among them, E_{total}, $E_{surface}$, and $E_{polymer}$ represent the total energy of the system, the surface energy of the substrate, and the energy of the adsorbate in the system, respectively, S represents the contact area, and E expresses the interfacial interaction energy. The smaller E indicates a more stable adsorption. SA, as a low surface energy material, can reduce the surface free energy. After calculation, the interaction energy of the acidified surface (-0.0317 kcal/mol/$Å^2$) is lower than that of the TiO_2 surface (-0.297 kcal/mol/$Å^2$). This means that the modification of SA molecules significantly reduces the adsorption of water molecular clusters on the surface, which also confirms the hydrophobic phenomenon. In addition, as shown in Figure 10, van der Waals force (-0.138 kcal/mol/
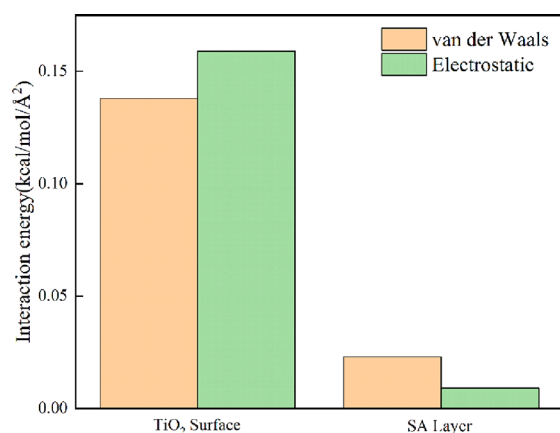
Figure 10. Interaction energy of different surface systems.

$Å^2$) and electrostatic force (-0.159 kcal/mol/$Å^2$) jointly dominate the adsorption of water molecules on the TiO_2 surface. For the SA-acidified surface, the contribution of van der Waals force (-0.0227 kcal/mol/$Å^2$) played a major role.

4. CONCLUSIONS

Organic modification of nano-TiO_2 by SA was carried out by a two-step spraying method. TiO_2 was successfully modified to superhydrophobicity, and the optimum preparation process was 0.3 g TiO_2. The hydrophobic mechanism was analyzed through the characterization of the modified nanoparticles and molecular dynamics simulation: SA reacted with the free hydroxyl on the surface of TiO_2 by the carboxyl group in the head, and the hydrophobic effect was achieved by the extremely long carbon chain of SA and the methyl and methylene groups in the tail. The concentration changes of the water layer on the surface of SiO_2 and TiO_2 were analyzed, and

the strong adsorption of water molecules on the two surfaces was verified. The hydrophilicity of the SiO_2 surface was slightly stronger than that of the TiO_2 surface. SA molecules can reduce the interfacial interaction energy in the system. The adsorption of water molecules on the TiO_2 surface is affected by van der Waals force and electrostatic force. van der Waals forces on the surface of SA acidification contributed most.

◾ AUTHOR INFORMATION

Corresponding Author

Xiaoru Hao − *School of Mechanical and Power Engineering, Henan Polytechnic University, Jiaozuo 454003, PR China;* ◎ orcid.org/0000-0001-6519-2929; Email: xiaoru408@ 126.com

Authors

Zhihao Cheng − *School of Mechanical and Power Engineering, Henan Polytechnic University, Jiaozuo 454003, PR China*

Yu Zhang − *School of Mechanical and Power Engineering, Henan Polytechnic University, Jiaozuo 454003, PR China*

Jun Xie − *School of Mechanical and Power Engineering, Henan Polytechnic University, Jiaozuo 454003, PR China*

Haikun Zheng − *School of Mechanical and Power Engineering, Henan Polytechnic University, Jiaozuo 454003, PR China*

Chunxiao Yue − *Shanghai Jian Qiao University, Shanghai 201306, PR China*

Wei Sheng − *School of Mechanical and Power Engineering, Henan Polytechnic University, Jiaozuo 454003, PR China; Hami Yuxin New Energy Industry Research Institute, Hami 839000, PR China*

Complete contact information is available at:
https://pubs.acs.org/10.1021/acsomega.3c07011

Notes

The authors declare no competing financial interest.

◾ REFERENCES

(1) Wei, Z.; Yang, B.; Zhao, M.; Yao, Y.; Gai, G. Preparation of Nano-SiO2/Fly Ash Microbeads Composite Particles by Hydrochloric Acid Precipitation Method. *J. China Univ. Min. Technol.* **2014**, *43*, 472.

(2) Nahum, T.; Dodiuk, H.; Dotan, A.; Kenig, S.; Lellouche, J. P. superhydrophobic Durable Coating Based on UV-Photoreactive Silica Nanoparticles. AIP Publishing LLC: United States 2015, *131*, DOI: 10.1063/1.4918436.

(3) Song, X.; Zhai, J.; Wang, Y.; Lei, J. Fabrication of superhydrophobic Surfaces by Self-assembly and Their Water-Adhesion Properties. *J. Phys. Chem. B* **2005**, *109*, 4048−4052.

(4) Xue, C. H.; Jia, S. T.; Zhang, J.; Ma, J. Z. Large-Area Fabrication of superhydrophobic Surfaces for Practical Applications: An Overview. *Sci. Technol. Adv. Mater.* **2010**, *11*, No. 033002.

(5) Subhash Latthe, S.; Basavraj Gurav, A.; Shridhar Maruti, C.; Shrikant Vhatkar, R. Recent Progress in Preparation of superhydrophobic Surfaces: A Review. *J. Surf. Eng. Mater. Adv. Technol.* **2012**, *2*, 76−94.

(6) Xu, W.; Song, J.; Sun, J.; Lu, Y.; Yu, Z. Rapid Fabrication of Large-Area, Corrosion-Resistant superhydrophobic Mg Alloy Surfaces. *ACS Appl. Mater. Interfaces.* **2011**, *3*, 4404−4414.

(7) She, Z.; Li, Q.; Wang, Z.; Tan, C.; Zhou, J.; Li, L. Highly Anticorrosion, Self-Cleaning superhydrophobic Ni-Co Surface Fabricated on AZ91D Magnesium Alloy. *Surf. Coat. Technol.* **2014**, *251*, 7−14.

(8) Suryaprabha, T.; Sethuraman, M. G. Fabrication of Copper-based superhydrophobic Self-Cleaning Antibacterial Coating over Cotton Fabric. *Cellulose* **2017**, *24*, 395−407.

(9) Asmone, A. S.; Chew, M. Y. L. An Investigation of superhydrophobic Self-Cleaning Applications on External Building Façade Systems in The Tropics. *J. Build. Eng.* **2018**, *17*, 167.

(10) Xue, C. H.; Guo, X. J.; Ma, J. Z.; Jia, S. T. Fabrication of Robust and Antifouling superhydrophobic Surfaces via Surface-Initiated Atom Transfer Radical Polymerization. *ACS Appl. Mater. Interfaces.* **2015**, *7*, 8251−8259.

(11) Li, W.; Zhang, Y.; Ding, J.; Zhang, S.; Hu, T.; Li, S.; et al. Temperature-triggered Fluorocopolymer Aggregate Coating Switching from Antibacterial to Antifouling and superhydrophobic Hemostasis. *Colloids and Surfaces B: Biointerfaces.* **2022**, *215*, No. 112496-.

(12) Lazauskas, A.; Guobienė, A.; Prosyčevas, I.; Baltrušaitis, V.; Grigaliūnas, V.; Narmontas, P.; Baltrušaitis, J. Water Droplet Behavior on superhydrophobic SiO_2 Nanocomposite Films during Icing/Deicing Cycles. *Mater. Charact.* **2013**, *82*, 9−16.

(13) Mishchenko, L.; Hatton, B.; Bahadur, V.; Taylor, J. A.; Krupenkin, T.; Aizenberg, J. Design of Ice-free Nanostructured Surfaces Based on Repulsion of Impacting Water Droplets. *ACS Nano* **2010**, *4*, 7699−7707.

(14) Alexander, S.; Eastoe, J.; Lord, A. M.; Guittard, F.; Barron, A. R. Branched Hydrocarbon Low Surface Energy Materials for super-hydrophobic Nanoparticle Derived Surfaces. *ACS Appl. Mater. Interfaces.* **2016**, *8*, 660−666.

(15) Bharathidasan, T.; Kumar, S. V.; Bobji, M. S.; Chakradhar, R.; Basu, B. J. Effect of Wettability and Surface Roughness on Ice-Adhesion Strength of Hydrophilic, Hydrophobic and superhydrophobic Surfaces. *Appl. Surf. Sci.* **2014**, *314*, 241−250.

(16) Liu, H.; Feng, L.; Zhai, J.; Jiang, L.; Zhu, D. Reversible Wettability of A Chemical Vapor Deposition Rrepared ZnO Film between Superhydrophobicity and Superhydrophilicity. *Langmuir.* **2004**, *20*, 5659−5661.

(17) Barshilia, H. C.; Gupta, N. superhydrophobic Polytetrafluoroethylene Surfaces with Leaf-Like Micro-Protrusions through Ar + O_2 Plasma Etching Process. *Vacuum.* **2014**, *99*, 42−48.

(18) Tadanaga, K.; Kitamuro, K.; Matsuda, A.; Minami, T. Formation of superhydrophobic Alumina Coating Films with High Transparency on Polymer Substrates by the Sol-gel Method. *J. Sol-gel Sci. Techn.* **2003**, *26*, 705−708.

(19) Lakshmi, R. V.; Bharathidasan, T.; Basu, B. J. superhydrophobic Sol-Gel Nanocomposite Coatings with Enhanced Hardness. *Appl. Surf. Sci.* **2011**, *257*, 10421−10426.

(20) Song, W.; Veiga, D. D.; Custódio, C. A.; Mano, J. F. Bioinspired Degradable Substrates with Extreme Wettability Properties. *Adv. Mater.* **2009**, *21*, 1830−1834.

(21) He, L. H.; Zhou, C.; Li, L.; Lu, Z. T. Superhydrophobicity of silane Coupling Agent Surface Modified Titanium Dioxide Particles. *Fine Chem.* **2014**, *31*, 1061−1064.

(22) Yang, F.; Cao, K. L.; Xu, Y. Y. Preparation and Characterization of stearic acid/TiO2/CNF superhydrophobic Composites. *China For. Prod. Ind.* **2019**, *46*, 5.

(23) Fumino, K.; Ludwig, R. Analyzing The Interaction Energies between Cation and Anion in Ionic Liquids: The Subtle Balance between Coulomb Forces and Hydrogen Bonding. *J. Mol. Liq.* **2014**, *192*, 94−102.

(24) Ueki, Y.; Matsuo, S.; Shibahara, M. Molecular Dynamic Study of Local Interfacial Thermal Resistance of Solid-Liquid and Solid-Solid Interfaces: Water and Nanotextured Surface. *International Communications in Heat and Mass Transfer.* **2022**, *137*, No. 106232.

(25) He, X.; Lou, T.; Cao, P.; Bai, X.; Yuan, C.; Wang, C.; Neville, A. Experimental and Molecular Dynamics Simulation Study of Chemically Stable superhydrophobic Surfaces. *Surf. Coat. Technol.* **2021**, *418*, No. 127236.

(26) Daneshmand, H.; Sazgar, A.; Araghchi, M. Fabrication of Robust and Versatile superhydrophobic Coating by Two-Step Spray Method: An Experimental and Molecular Dynamics Simulation Study. *Appl. Surf. Sci.* **2021**, *567*, No. 150825.

(27) Werder, T.; Walther, J. H.; Jaffe, R. L.; Halicioglu, T.; Noca, F.; Koumoutsakos, P. Molecular Dynamics Simulation of Contact Angles of Water Droplets in Carbon Nanotubes. *Nano Lett.* **2002**, *1*, 697.

(28) Gogotsi, Y.; Libera, J. A.; Guvenc-Yazicioglu, A.; Megaridis, C. M. In Situ Multiphase Fluid Experiments in Hydrothermal Carbon Nanotubes. *Appl. Phys. Lett.* **2001**, *79*, 1021.

(29) Rui, Z.; Xing, Y.; Xia, Y.; Luo, J.; Tan, J.; Rong, G.; Gui, X. New Insight into Surface Wetting of Coal with Varying Coalification Degree: An Experimental and Molecular Dynamics Simulation Study. *Appl. Surf. Sci.* **2020**, *511*, No. 145610.

(30) Ma, X.; Zheng, F.; Sittert, C. G. C. E. V.; Lu, Q. Role of Intrinsic Factors of Polyimides in Glass Transition Temperature: An Atomistic Investigation. *J. Phys. Chem. B* **2019**, *123*, 8569−8579.

(31) Song, X. Y.; Xing, X. L.; Zhao, S. X.; Ju, X. H. Molecular Dynamics Simulation on Tkx-50/Fluoropolymer. *Modell. Simul. Mater. Sci. Eng.* **2020**, *28*, No. 015004.